Charge-dependent calculations of single-particle energies in nuclei around ^{16}O with modern nucleon-nucleon interactions

Shinichiro Fujii*
Department of Physics, University of Tokyo, Tokyo 113-0033, Japan

Ryoji Okamoto and Kenji Suzuki
Department of Physics, Kyushu Institute of Technology, Kitakyushu 804-8550, Japan
(Received 15 November 2003; published 25 March 2004)

The binding energies of the ground states and several excited states related to single-particle and -hole states in nuclei around ^{16}O are calculated taking charge dependence into account. Effective interactions on the particle basis are constructed from modern charge-dependent nucleon-nucleon interactions and the Coulomb force within the framework of the unitary-model-operator approach. Single-particle (-hole) energies are obtained from the energy differences of the binding energies between a particle (hole) state in ^{17}O or ^{17}F (^{15}N or ^{15}O) and the ground state of ^{16}O. The resultant spin-orbit splittings are small for the hole state and large for the particle state in comparison with the experimental values though the differences between the experimental and calculated values are not very large. The charge dependence of the calculated single-particle energies for the ground states are in good agreement with the experimental values. Furthermore, the Thomas-Ehrman shift due to the Coulomb force for the $1s_{1/2}$ states in ^{17}O and ^{17}F can be observed.

DOI: 10.1103/PhysRevC.69.034328 PACS number(s): 21.30.Fe, 21.60.−n, 21.10.Pc, 27.20.+n

I. INTRODUCTION

The single-particle level is one of the fundamental structures in nuclei. Important physical quantities such as the spin-orbit splittings and the magic numbers are characterized by the single-particle level. Recently, it has been argued that some magic numbers disappear and new magic numbers arise in nuclei near the drip lines [1,2]. When we calculate the energies of single-particle levels in neutron- or proton-rich nuclei, it would be desirable that the calculation formalism is based on the particle basis. Advantages of the particle-basis formalism are that the Coulomb force can be treated accurately for the proton-proton channel and effects of charge dependence in realistic nuclear forces are taken into account in structure calculations. In the particle-basis formalism, one can obtain the energy differences between proton and neutron levels for not only $N=Z$ nuclei but also neutron- or proton-rich nuclei in the same manner.

The calculation of single-particle energies starting with a nucleon-nucleon force in free space is a fundamental problem in theoretical nuclear physics. There have been many attempts to understand the structure of single-particle levels as well as other ground-state properties in nuclei [3–7]. In such calculations, we need a many-body theory that leads to an effective interaction in a restricted model space for a nucleus in many cases. For this purpose, the G matrix has been widely used as a basic ingredient in performing structure calculations [8,9]. A recent study of the doubly closed-shell nucleus ^{16}O using the G matrices constructed from modern nucleon-nucleon interactions can be seen in Ref. [10]. Lately, as an alternative of the G matrix, a low-momentum potential $V_{\text{low-}k}$ has been constructed from a realistic nucleon-nucleon interaction using a renormalization group technique or conventional effective interaction theory by Bogner *et al.* [11]. The application of $V_{\text{low-}k}$ to the calculation of ground-state properties of the closed-shell nuclei ^{16}O and ^{40}Ca has been done in Ref. [12].

As one of the methods for solving nuclear many-body problems, we have developed the unitary-model-operator approach (UMOA) [13]. An energy-independent and Hermitian effective interaction is derived through a unitary transformation of an original Hamiltonian. Nuclear ground-state properties, such as the ground-state energy, charge radius, and single-particle energy have been calculated for ^{16}O [14] and ^{40}Ca [15]. We have learned that spin-orbit splittings for hole states are enlarged by taking second-order diagrams into account. Furthermore, the UMOA has been developed for the structure calculation of Λ hypernuclei and applied to $^{16}_{\Lambda}$O, $^{17}_{\Lambda}$Ca, and $^{41}_{\Lambda}$Ca using hyperon-nucleon interactions in free space [16,17]. Differences in the properties of modern hyperon-nucleon interactions have been disclosed in the structure calculation.

Recently, we have extended the formulation of the UMOA from the isospin basis to the particle one for the purpose of the charge-dependent calculation. To confirm the validity of the calculation method based on the particle basis, in this paper, we apply this method to ^{16}O and its neighboring nuclei ^{15}N, ^{15}O, ^{17}O, and ^{17}F. Binding energies of these nuclei are calculated for the ground states, and excited states which have the single-particle or single-hole structure as the main component. The single-particle energy in the neighboring nuclei is given as the relative energy between a single-particle (-hole) state in the neighboring nuclei and the ground state of ^{16}O. As for the single-particle (-hole) state, the excitation up to two-particle one-hole (one-particle two-hole) from the unperturbed ground state of ^{16}O are taken into account.

*Electronic address: sfujii@nt.phys.s.u-tokyo.ac.jp

Four high-precision nucleon-nucleon interactions represented in momentum space are employed, namely, the Nijmegen 93 (Nijm 93) [18], Nijm I [19], the charge-dependent Bonn (CD Bonn) [20], and the next-to-next-to-next-to-leading order (N^3LO) potential [21] based on chiral perturbation theory [22,23] which has recently been constructed by Entem and Machleidt. In these potentials, effects of charge dependence are taken into account. The first three potentials are based on meson-exchange models in which several kinds of meson are incorporated. On the other hand, the essential degrees of freedom of the mesons in the N^3LO potential are only for the pions. Therefore, the N^3LO potential is constructed in a low-momentum region compared to the meson-exchange potentials which have heavier mesons. However, the N^3LO potential has the high accuracy to reproduce the nucleon-nucleon data below $E_{\rm lab}=290$ MeV, and thus the N^3LO potential as well as other high-precision nucleon-nucleon interactions can be used in nuclear structure calculations.

This paper is organized as follows. In Sec. II, the methods for deriving effective interactions and performing structure calculations are given. In Sec. III, calculated results for ^{16}O and its neighboring nuclei using the four realistic interactions are presented. Finally, we summarize the present work in Sec. IV.

II. METHOD OF CALCULATION

In the UMOA, the Hamiltonian to be considered is given by a cluster expansion of a unitarily transformed Hamiltonian. In the previous works [13,14], many-body correlations up to three-body cluster terms have been evaluated. It has been confirmed that the cluster expansion in the numerical calculation for ^{16}O shows the good convergence at the three-body cluster level. We may say that since we consider the $N \simeq Z$ nuclei around ^{16}O in the present study, the three-body cluster terms do not have a significant contribution to the energy difference between the single-particle (-hole) levels of the proton and neutron. Therefore, in the present calculation, we neglect the three-body cluster terms for simplicity. The evaluation of the three-body cluster terms based on the particle basis is a further challenge which should be accomplished for a deeper understanding of nuclei.

In the following sections, we present a general framework for deriving an effective interaction and a practical method for the structure calculation in the present study.

A. Derivation of effective interaction in the *P* and *Q* spaces

In the usual sense of effective interaction theory, an effective interaction is defined in a low-momentum model space (P space). However, in general, one can also derive an effective interaction in the complement (Q space) of the P space by making the decoupling condition for the effective interaction $\tilde{v}$ as $Q\tilde{v}P=0$. Note that the projection operators P and Q satisfy the usual relations as $P+Q=1$, $P^2=P$, $Q^2=Q$, and $PQ=QP=0$. We here present a general framework for deriving a two-body effective interaction of Hermitian type for a two-body system.

The two-body effective interaction $\tilde{v}_{12}$ of Hermitian type is written as

$$\tilde{v}_{12} = U^{-1}(h_0 + v_{12})U - h_0, \tag{1}$$

where v_{12} is the bare two-body interaction and h_0 is the one-body part of the two-body system which consists of the kinetic energy $t_1(t_2)$ and, if necessary, the single-particle potential $u_1(u_2)$ as $h_0=t_1+u_1+t_2+u_2$. The operator U for the unitary transformation of h_0+v_{12} can be written as [24]

$$U = (1 + \omega - \omega^\dagger)(1 + \omega\omega^\dagger + \omega^\dagger\omega)^{-1/2} \tag{2}$$

by introducing the operator ω satisfying $\omega=Q\omega P$ and thus $\omega^2=\omega^{\dagger 2}=0$. The above expression of U agrees with the block form using the projection operators P and Q of kubo [25] given by

$$U = \begin{pmatrix} P(1 + \omega^\dagger\omega)^{-1/2}P & -P\omega^\dagger(1 + \omega\omega^\dagger)^{-1/2}Q \\ Q\omega(1 + \omega^\dagger\omega)^{-1/2}P & Q(1 + \omega\omega^\dagger)^{-1/2}Q \end{pmatrix}. \tag{3}$$

We should note here that the operator U is also expressed as

$$U = e^S, \tag{4}$$

where S is anti-Hermitian and given under the restrictive conditions $PSP=QSQ=0$ by

$$S = \operatorname{arctanh}(\omega - \omega^\dagger). \tag{5}$$

In order to obtain the matrix elements of ω, we first solve exactly the two-body eigenvalue equation as

$$(h_0 + v_{12})|\Phi_k\rangle = E_k|\Phi_k\rangle. \tag{6}$$

With the eigenvector $|\Phi_k\rangle$, the matrix elements of ω on the basis states $|p\rangle$ in the P space and $|q\rangle$ in the Q space can be determined as

$$\langle q|\omega|p\rangle = \sum_{k=1}^{d} \langle q|Q|\Phi_k\rangle\langle\tilde{\phi}_k|p\rangle, \tag{7}$$

where d is the dimension of the P space and $\langle\tilde{\phi}_k|$ is the biorthogonal state of $|\phi_k\rangle=P|\Phi_k\rangle$, which means the matrix inversion $[\langle\tilde{\phi}_k|p\rangle]=[\langle p'|\phi_k\rangle]^{-1}$ and satisfies $\Sigma_p \langle\tilde{\phi}_k|p\rangle\langle p|\phi_{k'}\rangle=\delta_{k,k'}$ and $\Sigma_k \langle p'|\tilde{\phi}_k\rangle\langle\phi_k|p\rangle=\delta_{p,p'}$. It should be noted that the set of eigenstates $\{|\Phi_k\rangle, k=1,2,\ldots,d\}$ is selected so that they have the largest P-space overlaps among all the eigenstates in Eq. (6).

Then, in order to obtain the matrix elements of U, we introduce the eigenvalue equation for $\omega^\dagger\omega$ in the P space as

$$\omega^\dagger\omega|\alpha_k\rangle = \mu_k^2|\alpha_k\rangle. \tag{8}$$

Using the solutions to the above equation, we define the ket vector $|\nu_k\rangle$ as

$$|\nu_k\rangle = \frac{1}{\mu_k}\omega|\alpha_k\rangle, \tag{9}$$

which is also written as

$$\langle q|\nu_k\rangle = \frac{1}{\mu_k}\sum_p \langle q|\omega|p\rangle\langle p|\alpha_k\rangle. \tag{10}$$

Using Eqs. (8)–(10), we obtain the matrix elements of the unitary-transformation operator U in Eq. (2) as

$$\langle p'|U|p\rangle = \langle p'|(1+\omega^\dagger\omega)^{-1/2}|p\rangle = \sum_{k=1}^{d}(1+\mu_k^2)^{-1/2}\langle p'|\alpha_k\rangle\langle\alpha_k|p\rangle, \tag{11}$$

$$\langle q|U|p\rangle = \langle q|\omega(1+\omega^\dagger\omega)^{-1/2}|p\rangle = \sum_{k=1}^{d}(1+\mu_k^2)^{-1/2}\mu_k\langle q|\nu_k\rangle\langle\alpha_k|p\rangle, \tag{12}$$

$$\langle p|U|q\rangle = -\langle p|\omega^\dagger(1+\omega\omega^\dagger)^{-1/2}|q\rangle = -\sum_{k=1}^{d}(1+\mu_k^2)^{-1/2}\mu_k\langle p|\alpha_k\rangle\langle\nu_k|q\rangle, \tag{13}$$

and

$$\langle q'|U|q\rangle = \langle q'|(1+\omega\omega^\dagger)^{-1/2}|q\rangle = \sum_{k=1}^{d}\{(1+\mu_k^2)^{-1/2}-1\}\langle q'|\nu_k\rangle\langle\nu_k|q\rangle + \delta_{q,q'}. \tag{14}$$

Thus, the matrix elements of the effective interaction $\tilde{v}_{12}$ in Eq. (1) can be written as

$$\langle i|\tilde{v}_{12}|j\rangle = \sum_{k,l}\langle i|U^{-1}|k\rangle\langle k|h_0+v_{12}|l\rangle\langle l|U|j\rangle - \langle i|h_0|j\rangle, \tag{15}$$

where $|i\rangle$, $|j\rangle$, $|k\rangle$, and $|l\rangle$ denote the basis states in the $P+Q$ space.

The above formulation is employed for deriving the effective interaction in the present study. Here we note that since we treat a many-body system, the single-particle potential u_1 (u_2) in h_0 for both particle and hole states is introduced to obtain a good unperturbed energy. In the following, a procedure for determining the effective interaction and the single-particle potential is given.

B. Two-step method for the calculation of effective interaction

In nuclear many-body problems, how to determine the single-particle potential for particle (unoccupied) states as well as hole (occupied) states is important in connection with the evaluation of many-body correlations [26–29]. In our calculations, the single-particle potential, which is determined self-consistently with the two-body effective interaction, is calculated up to a sufficiently high-momentum region. In general, this choice of the single-particle potential leads to a deeper binding of the ground-state energy of a nucleus in the lowest order. Then, effects of the many-body correlations of higher order become smaller than the choice of only the kinetic energy for the particle state. This trend would be favorable when the evaluation of many-body correction terms has to be limited in the actual calculation.

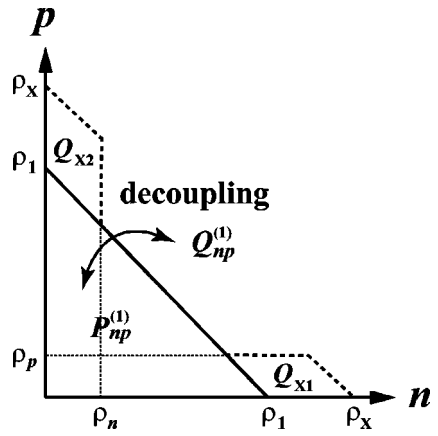

FIG. 1. Model space $P_{np}^{(1)}$ and its complement $Q_{np}^{(1)}$ for the np channel in the first-step calculation.

In our earlier calculations, the effective interaction was derived by a three-step procedure with some approximations to take account of single-particle potentials up to a high-momentum region. In the present work, however, we adopt a two-step procedure and approximation methods are refined, because the performance of the computer has been greatly improved and some approximations in the previous works are not needed at present. In the following, we shall give the two-step procedure for the numerical calculation.

1. First-step calculation

In this work, we employ the harmonic-oscillator (ho) wave functions as the basis states. Two-nucleon states for $Z=nn$, np, pp channels consisting of the product of the ho states are given by

$$|\alpha\beta\rangle_Z = |n_a l_a j_a m_a, n_b l_b j_b m_b\rangle_Z. \tag{16}$$

The model space $P_Z^{(1)}$ and its complement $Q_Z^{(1)}$ composed of the two-nucleon states for the Z channel are defined with a boundary number ρ_1 as

$$|\alpha\beta\rangle_Z \in \begin{cases} P_Z^{(1)} & \text{if } 2n_a+l_a+2n_b+l_b \leqslant \rho_1 \\ Q_Z^{(1)} & \text{otherwise,} \end{cases} \tag{17}$$

which is also illustrated only for the np channel in Fig. 1. The nn and pp channels are considered similarly in the actual calculation. The value of ρ_1 is taken as large as possible so that the calculated results do not depend on this value. The ρ_1 dependence of calculated results will be investigated in Sec. III. The symbols ρ_n and ρ_p in Fig. 1 stand for the uppermost occupied states of the neutron and proton, respectively, and in the present case of ^{16}O, ρ_n and ρ_p are the $0p_{1/2}$ orbits. The Q_{X1} and Q_{X2} spaces defined with ρ_1, ρ_n, ρ_p, and ρ_X in the $Q_{np}^{(1)}$ space should be excluded due to the Pauli principle when we calculate matrix elements of the bare two-body interaction. The value of ρ_X is determined so that the Pauli principle from the states in the Q_{X1} and Q_{X2} spaces can well be taken into account, and taken as $\rho_X=2n_a+l_a+2n_b+l_b=20$ in the present study.

It is noted that, in this first step, the effective interaction is constructed using the relative and center-of-mass (c.m.) states of the ho wave functions. Since we consider a huge Hilbert space, it is very difficult to use the basis states composed of the product of the single-particle ho states in the model and complementary spaces. In the following, we shall give a practical method for calculating the effective interaction and the single-particle potential. In order to derive the two-body effective interaction for each of $Z=nn$, np, pp channels we rewrite Eq. (6) in terms of the relative and c.m. states as

$$\begin{aligned}&[P_Z^{(1)}\{t_r+u_{12}(N,L)\}P_Z^{(1)}+Q_Z^{(1)}t_rQ_Z^{(1)}+t_{\mathrm{c.m.}}\\&\quad+(P_Z^{(1)}+\overline{Q}_Z^{(1)})v_{12}(P_Z^{(1)}+\overline{Q}_Z^{(1)})]|k;l(l')SJ_r,NL\rangle_Z\\&=E_k|k;l(l')SJ_r,NL\rangle_Z,\end{aligned}\tag{18}$$

where $l(l')$ and S are the orbital angular momentum and spin of a relative state, and J_r is the total angular momentum given by $\mathbf{J}_r=\mathbf{l}+\mathbf{S}$. The letter k means an additional quantum number specifying an eigenstate. The terms t_r and $t_{\mathrm{c.m.}}$ are the kinetic energies of the relative and c.m. motions, respectively, and v_{12} is the bare interaction. The operator $\overline{Q}_Z^{(1)}$ projects two-body states on to the $Q_Z^{(1)}$ space, but Pauli-forbidden two-body states in the Q_{X1} and Q_{X2} spaces are excluded. The sum of two single-particle potentials in the relative and c.m. states is denoted by $u_{12}(N,L)$. We assume, in the present study, that the matrix elements in solving Eq. (18) are diagonal in each of the c.m. quantum numbers N and L. Thus, the resultant effective interaction becomes also diagonal in the c.m. quantum numbers.

The matrix elements of $u_{12}(N,L)$ can be written under the angle-average approximation [14,30] as

$$\begin{aligned}&\langle nlS\,J_r,NL|u_{12}(N,L)|n'l'S\,J_r,NL\rangle_Z\\&=\delta_{l,l'}\sum_{\substack{n_an'_al_aj_an_bl_bj_b\\ \lambda\lambda' J}}(-1)^{\lambda+\lambda'}\\&\quad\times\begin{Bmatrix}l_a&\frac{1}{2}&j_a\\ l_b&\frac{1}{2}&j_b\\ \lambda&S&J\end{Bmatrix}\begin{Bmatrix}l_a&\frac{1}{2}&j_a\\ l_b&\frac{1}{2}&j_b\\ \lambda'&S&J\end{Bmatrix}\\&\quad\times\frac{[\lambda][\lambda'][j_a][j_b][S][J]}{[L]}W(LlJS;\lambda J_r)W(Ll'JS;\lambda' J_r)\\&\quad\times\langle nlNL\lambda|n_al_an_bl_b\lambda\rangle\langle n'l'NL\lambda'|n'_al_an_bl_b\lambda'\rangle\\&\quad\times(\langle n_al_aj_a|u_{z_1}^{(1)}|n'_al_aj_a\rangle+\langle n_al_aj_a|u_{z_2}^{(1)}|n'_al_aj_a\rangle),\end{aligned}\tag{19}$$

where $[x]\equiv 2x+1$ and J is the total angular momentum for two single-particle ho states given by $\mathbf{J}=\mathbf{j_a}+\mathbf{j_b}$. The coefficients $\{\cdots\}$, $W(\cdots)$, and $\langle nl\cdots|n_al_a\cdots\rangle$ denote the Wigner 9-j symbols, the Racah coefficients, and the ho transformation brackets, respectively. Note that, as for the nn and pp channels, the calculation should be done only for $l+S=$even. The quantities $u_{z_1}^{(1)}$ and $u_{z_2}^{(1)}$ represent the single-particle potentials of the neutron $u_n^{(1)}$ or proton $u_p^{(1)}$ in the first-step calculation, depending on $Z=nn$, np, pp channels. The single-particle potentials $u_n^{(1)}$ and $u_p^{(1)}$ are calculated self-consistently with the two-body effective interaction, which will be shown later.

The operator $\overline{Q}_Z^{(1)}$ can be written under the angle-average approximation as

$$\overline{Q}_Z^{(1)}=\sum_{\substack{nlNLSJ_r\\ \rho_1<2n+l+2N+L}}\theta_Z(n,l,N,L,S,J_r)|nlSJ_r,NL\rangle\langle nlSJ_r,NL|,\tag{20}$$

where

$$\begin{aligned}&\theta_Z(n,l,N,L,S,J_r)\\&=1-\sum_{\substack{ab\lambda\lambda' J\\ \rho_1<2n_a+l_a+2n_b+l_b\le\rho_X}}(-1)^{\lambda+\lambda'}f_Z\\&\quad\times\begin{Bmatrix}l_a&\frac{1}{2}&j_a\\ l_b&\frac{1}{2}&j_b\\ \lambda&S&J\end{Bmatrix}\begin{Bmatrix}l_a&\frac{1}{2}&j_a\\ l_b&\frac{1}{2}&j_b\\ \lambda'&S&J\end{Bmatrix}\\&\quad\times\frac{[\lambda][\lambda'][j_a][j_b][S][J]}{[L]}W(LlJS;\lambda J_r)W(Ll'JS;\lambda' J_r)\\&\quad\times\langle nlNL\lambda|n_al_an_bl_b\lambda\rangle\langle nlNL\lambda'|n_al_an_bl_b\lambda'\rangle\end{aligned}\tag{21}$$

with

$$f_Z=\begin{cases}2\text{ for }Z=nn\text{ or }pp\\ 1\text{ for }Z=np.\end{cases}\tag{22}$$

Note that, as for the nn and pp channels, the calculation should be done only for $l+S=$even. The letter a (b) for the summation in Eq. (21) means a set of the quantum numbers $a\equiv\{n_a,l_a,j_a,z=n\text{ or }p\}$ of a single-particle ho state. The conditions of the summation of single-particle states a and b for the nn and pp channels are $\{a\le\rho_n,b>\rho_n\}$ and $\{a\le\rho_p,b>\rho_p\}$, respectively. As for the np channel, $\{a\le\rho_n,b>\rho_p\}$ or $\{a>\rho_n,b\le\rho_p\}$. Here for example, the notation $\{a\le\rho_n,b>\rho_p\}$ for the np channel means that the summation is done for occupied states of the neutron and unoccupied states of the proton.

It should be noted that Eq. (18) is solved exactly by diagonalizing the matrix elements of several hundred coordinate-space ho basis states for each channel on the assumption of the diagonal c.m. quantum numbers. If we employ a bare interaction in momentum-space representation, the Fourier transformation for the ho wave function is needed in calculating the matrix elements of the bare interaction. Using the eigenvector $|k;l(l')SJ_r,NL\rangle_Z$, the operator ω in Eq. (7) can be written in terms of relative and c.m. states. Then, the matrices of the effective interaction $\tilde{v}_{12}^{(1)}$ in Eq. (15) are obtained in the relative and c.m. states as $\langle nlSJ_r|\tilde{v}_{12}(N,L)|n'l'SJ_r\rangle_Z$ through Eqs. (7)–(15). Note that we do not need the Q-space effective interaction in the first-step calculation if we take a sufficiently large model space.

The transformation of the effective interaction in the relative and c.m. states into the one in the shell-model states can be performed straightforwardly as

$$\langle ab|\tilde{v}_{12}^{(1)}|cd\rangle_{J,Z} = \frac{1}{\sqrt{1+\delta_{a,b}}}\frac{1}{\sqrt{1+\delta_{c,d}}}\sum_{\substack{nln'l'J_rS\\ NL\lambda\lambda'}}(-1)^{\lambda+\lambda'} f_Z(l,S)$$
$$\times\sqrt{[j_a][j_b][j_c][j_d]}[\lambda][\lambda'][S][J_r]$$
$$\times\begin{Bmatrix} l_a & \frac{1}{2} & j_a \\ l_b & \frac{1}{2} & j_b \\ \lambda & S & J \end{Bmatrix}\begin{Bmatrix} l_c & \frac{1}{2} & j_c \\ l_d & \frac{1}{2} & j_d \\ \lambda' & S & J \end{Bmatrix}$$
$$\times W(LlJS;\lambda J_r)W(Ll'JS;\lambda' J_r)$$
$$\times\langle nlNL\lambda|n_a l_a n_b l_b\lambda\rangle\langle n'l'NL\lambda'|n_c l_c n_d l_d\lambda'\rangle$$
$$\times\langle nlSJ_r|\tilde{v}_{12}^{(1)}(N,L)|n'l'SJ_r\rangle_Z, \qquad (23)$$

where

$$f_Z(l,S) = \begin{cases} 1+(-1)^{l+S} & \text{for } Z=nn \text{ or } pp \\ 1 & \text{for } Z=np, \end{cases} \qquad (24)$$

which is required for the antisymmetrization of the matrix elements in the shell-model states. Note that $l+S$=even for the *nn* and *pp* channels.

The single-particle potentials $u_{z_1}^{(1)}$ and $u_{z_2}^{(1)}$ in Eq. (19) are determined self-consistently with the two-body effective interaction $v_{12}^{(1)}$, which is written as

$$\langle a|u_n^{(1)}|a'\rangle = \sum_{\substack{J,Z=nn,np\\ m:\text{occupied}}}\frac{1}{\sqrt{1+\delta_{a,m}}}\frac{1}{\sqrt{1+\delta_{a',m}}}(2J+1)$$
$$\times\langle am|\tilde{v}_{12}^{(1)}|a'm\rangle_{J,Z} \qquad (25)$$

for the neutron and

$$\langle a|u_p^{(1)}|a'\rangle = \sum_{\substack{J,Z=pp,np\\ m:\text{occupied}}}\frac{1}{\sqrt{1+\delta_{a,m}}}\frac{1}{\sqrt{1+\delta_{a',m}}}(2J+1)$$
$$\times\langle ma|\tilde{v}_{12}^{(1)}|ma'\rangle_{J,Z} \qquad (26)$$

for the proton.

The procedure for the self-consistent calculation is as follows. First, we input initial values of $u_{z_1}^{(1)}$ and $u_{z_2}^{(1)}$ in Eq. (19), and solve the eigenvalue equation in Eq. (18) for each of $Z=nn$, *np*, *pp* channels. Through Eqs. (7)–(15), the effective interaction in the form of the reduced matrix element is determined. Then, the new single-particle potentials are calculated through Eqs. (23)–(26). These new values of the single-particle potentials are used in Eq. (19), and the iterative calculation is performed until the calculated results converge.

We remark here that one of the practical methods of the structure calculations using the present effective interaction would be the shell-model diagonalization. However, the application of such a calculation may be limited only to light nuclei, because we must take account of many single-particle states in the model space and the dimension of the matrices to be diagonalized becomes very huge. Since we intend to obtain only the energies of the ground state of the closed-shell nucleus and the single-particle (-hole) states in its neighboring nuclei, we proceed to the next step for a more practical calculation. In the second-step calculation, the effective interaction determined in the first-step calculation is unitarily transformed again so that the matrix elements for two-particle two-hole ($2p2h$) excitation reduce to zero. This is an essential point of the UMOA. By virtue of this, a number of many-body correlations with the vertices of the effective interaction are reduced compared to the usual linked-cluster expansion with the *G* matrix. In the UMOA, such many-body correlations can be evaluated in a cluster expansion of the unitarily transformed Hamiltonian with the vertices of *S* in Eq. (5), the one-body Hamiltonian, and the two-body effective interaction.

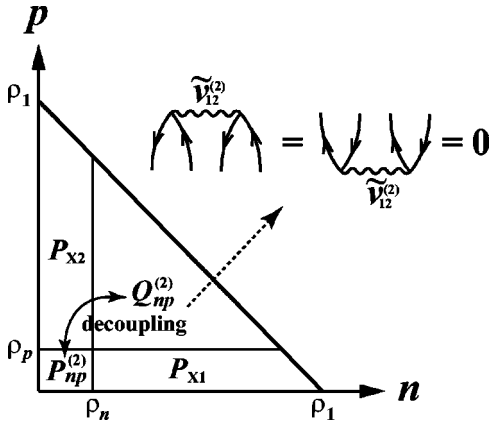

FIG. 2. Model space $P_{np}^{(2)}$ and its complement $Q_{np}^{(2)}$ for the *np* channel in the second-step calculation.

2. Second-step calculation

Using the two-body effective interaction $\tilde{v}_{ij}^{(1)}$ determined in the first-step calculation, we consider the internal Hamiltonian as

$$\tilde{H}_{\text{int}} = \sum_i t_i + \sum_{i<j}\tilde{v}_{ij}^{(1)} - T_{\text{c.m.}}, \qquad (27)$$

where $T_{\text{c.m.}}$ is the kinetic energy of the c.m. motion. In this second step, the calculations are performed using the basis states of the product of the single-particle ho states. In order to remove spurious c.m. states, we add the c.m. Hamiltonian

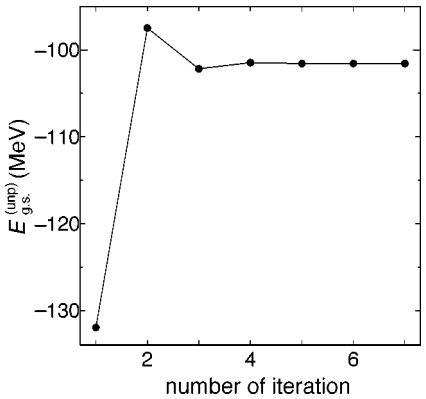

FIG. 3. Convergence of the unperturbed ground-state energy for the iterative calculation for ^{16}O in the second-step calculation for $\rho_1=12$ and $\hbar\Omega=14$ MeV. The CD-Bonn potential is employed.

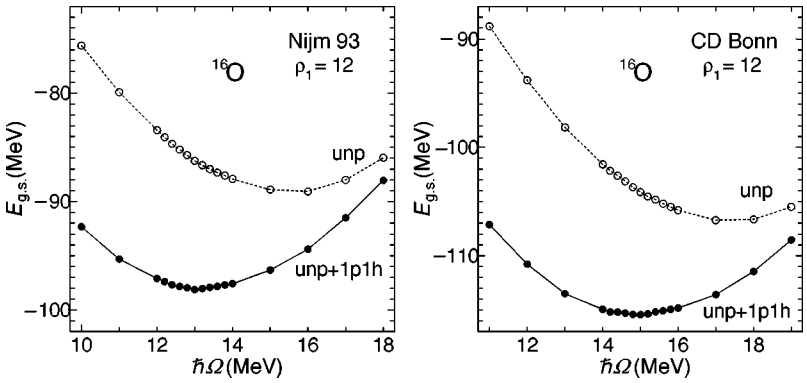

FIG. 4. The $\hbar\Omega$ dependence of calculated ground-state energies of ^{16}O for $\rho_1=12$ for the Nijm-93 and the CD-Bonn potentials.

$H_{\text{c.m.}}$ so as to constrain the ground-state c.m. motion in the ho potential with the frequency Ω as

$$H_{\text{c.m.}} = \beta_{\text{c.m.}}\left(T_{\text{c.m.}} + U_{\text{c.m.}} - \frac{3}{2}\hbar\Omega\right). \tag{28}$$

The ho potential $U_{\text{c.m.}}$ can be written with the mass number A and the nucleon mass m as

$$U_{\text{c.m.}} = \tfrac{1}{2}Am\,\Omega^2\mathbf{R}^2 = \sum_{i<j}\left(\frac{1}{A-1}X_{ij} - \frac{A-2}{A(A-1)}x_{ij}\right), \tag{29}$$

where $X_{ij}=\frac{1}{2}(2m)\Omega^2\mathbf{R}_{ij}^2$ and $x_{ij}=\frac{1}{2}(m/2)\Omega^2\mathbf{r}_{ij}^2$. The definitions of the coordinates are $\mathbf{R}=(1/A)\Sigma_i\,\mathbf{r}_i$, $\mathbf{R}_{ij}=\frac{1}{2}(\mathbf{r}_i+\mathbf{r}_j)$, and $\mathbf{r}_{ij}=\mathbf{r}_i-\mathbf{r}_j$. We assume that the nucleon mass is the mean value of the neutron and proton. As for the value of $\beta_{\text{c.m.}}$ in Eq. (28), in the present study, we simply take as $\beta_{\text{c.m.}}=1$ which could be acceptable as discussed in Refs. [31,32]. Thus, the Hamiltonian to be considered in the second-step calculation becomes

$$\tilde{H} = H_{\text{int}} + H_{\text{c.m.}} = \sum_i t_i + \sum_{i<j}\tilde{V}_{ij}^{(1)}(A) - \frac{3}{2}\hbar\Omega, \tag{30}$$

where

$$\tilde{V}_{ij}^{(1)}(A) = \tilde{v}_{ij}^{(1)} + \frac{1}{A-1}X_{ij} - \frac{A-2}{A(A-1)}x_{ij}. \tag{31}$$

Note that the above two-body interaction is A dependent.

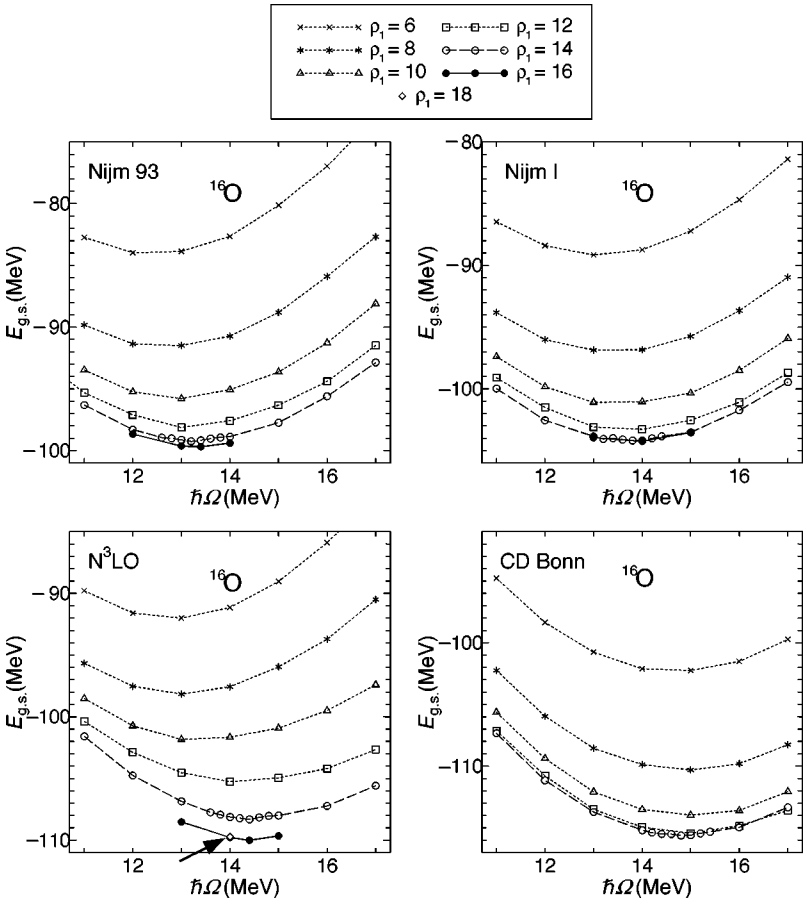

FIG. 5. The $\hbar\Omega$ and ρ_1 dependences of calculated ground-state energies with the $1p1h$ effect of ^{16}O for various modern nucleon-nucleon interactions.

TABLE I. The calculated ground-state energies with the $1p1h$ effect and the binding energies per nucleon of ^{16}O. In these calculated values, the optimal values of $\hbar\Omega$ for each interaction are employed. As for the value of ρ_1, we take as $\rho_1=14$ for the CD Bonn and $\rho_1=16$ for the other interactions as the sufficiently large value as suggested in Fig. 5. The experimental values are taken from Ref. [34]. All energies are in MeV.

^{16}O	Nijm 93	Nijm I	N^{3}LO	CD Bonn	Expt.
$E_{\text{g.s.}}$	−99.69	−104.25	−110.00	−115.61	−127.62
BE/A	6.23	6.52	6.88	7.23	7.98

The central aim of the present study is to calculate the binding energies of the ground state of ^{16}O and its neighboring nuclei, and to obtain single-particle energies using the Hamiltonian in Eq. (30). To accomplish this without performing the full shell-model diagonalization, we proceed to the decoupling calculation again. The model space in the first-step calculation in Fig. 1 is separated as shown in Fig. 2. The *model* space and its *complement* for the *np* channel are denoted by $P_{np}^{(2)}$ and $Q_{np}^{(2)}$, respectively. It should be noted that we solve the *P*-space and *Q*-space problems on an equal footing in the second-step calculation, using the effective interaction determined in the first-step calculation which has already incorporated the effect of the short-range correlation of the bare interaction. The P_{X1} and P_{X2} spaces are the Pauli-blocked spaces in the second-step calculation.

It would be worthy to mention the property of the effective interaction to be determined in the second-step calculation. By taking the model and complementary spaces as shown in Fig. 2, the resultant effective interaction $\tilde{v}_{12}^{(2)}$ which is determined from the decoupling condition $Q_Z^{(2)}\tilde{v}_{12}^{(2)}P_Z^{(2)}=0$ for $Z=nn$, np, pp has no vertices which induce $2p2h$ excitation. This is analogous to the Hartree-Fock (HF) condition which means that an original Hamiltonian is transformed so that the matrix elements for $1p1h$ excitation reduce to zero. Although the vertices of the one-body nondiagonal matrix elements remain in determining the effective interaction, these nondiagonal matrix elements are diagonalized at the end of the calculation.

The eigenvalue equation for the Z channel in the second-step calculation which corresponds to Eq. (6) can be written as

$$\{t_{z_1}+u_{z_1}^{(2)}+t_{z_2}+u_{z_2}^{(2)}+\tilde{V}_{12}^{(1)}(A)\}|\Psi_k\rangle_{J^\pi,Z}=E_k|\Psi_k\rangle_{J^\pi,Z}, \tag{32}$$

where $|\Psi_k\rangle_{J^\pi,Z}$ represents a two-body eigenstate in terms of the basis states of the product of the single-particle ho states with a good total angular momentum and parity for the Z channel. We solve the above eigenvalue equation exactly by diagonalizing the matrix elements in the *full* space $P_Z^{(2)}+Q_Z^{(2)}$, and then obtain the matrix elements of U in this full space through Eqs. (7)–(14). In addition, the matrix elements of U for the P_{X1} and P_{X2} spaces are given by

$$\langle x'|U|x\rangle=\delta_{x,x'} \tag{33}$$

and

$$\langle p|U|x\rangle=\langle q|U|x\rangle=\langle x|U|p\rangle=\langle x|U|q\rangle=0, \tag{34}$$

where $|x\rangle$, $|p\rangle$, and $|q\rangle$ are the basis states in the P_{X1} and P_{X2}, $P_Z^{(2)}$, and $Q_Z^{(2)}$ spaces, respectively.

The calculation procedure in the second step is as follows. We first solve exactly Eq. (32) by the diagonalization. As the initial values of $u_{z_1}^{(2)}$ and $u_{z_2}^{(2)}$ in Eq. (32), we use the single-particle potentials determined in the first-step calculation. Through Eqs. (7)–(15), the effective interaction $\tilde{v}_{12}^{(2)}$ in this second step in all the P_{X1}, P_{X2}, $P_Z^{(2)}$, and $Q_Z^{(2)}$ spaces is determined. Then, the single-particle potentials $u_n^{(2)}$ and $u_p^{(2)}$ are calculated in Eqs. (25) and (26) using the effective interaction $\tilde{v}_{12}^{(2)}$ instead of $\tilde{v}_{12}^{(1)}$ determined in the first step, and the self-consistent calculation is performed iteratively until the calculated results converge.

As a typical example of the convergence of the self-consistent calculation, in Fig. 3, we show the results of the unperturbed ground-state energy of ^{16}O in the second-step calculation with increasing number of iteration for $\rho_1=12$ with the CD-Bonn potential. The Coulomb interaction is included in the calculation. The unperturbed ground-state energy $E_{\text{g.s.}}^{(\text{unp})}$ of the doubly closed-shell nucleus is given by

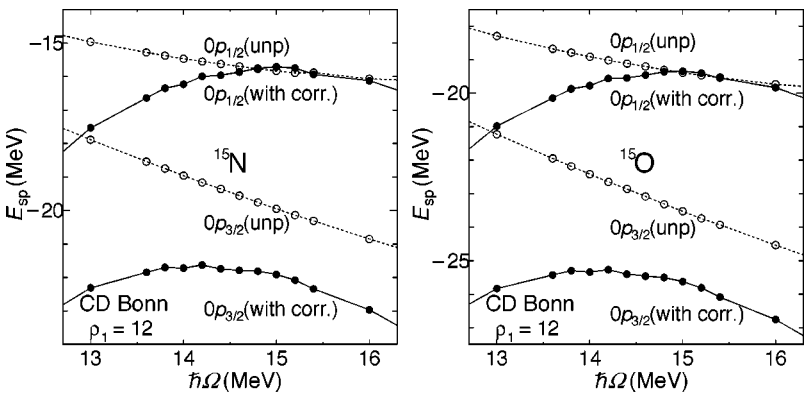

FIG. 6. The $\hbar\Omega$ dependence of calculated single-particle energies for $\rho_1=12$ for hole states in ^{16}O. The left (right) figure is for the proton (neutron) levels which correspond to the single-hole states in ^{15}N (^{15}O). The CD-Bonn potential is employed.

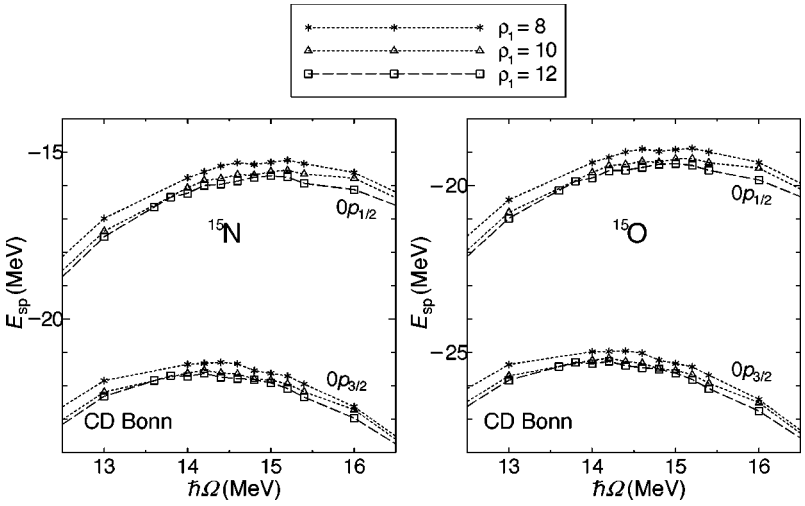

FIG. 7. The $\hbar\Omega$ and ρ_1 dependences of calculated single-particle energies with the $1p2h$ effect for the proton (^{15}N) and neutron (^{15}O) levels. The CD-Bonn potential is employed.

$$E_{\text{g.s.}}^{(\text{unp})} = \sum_{\substack{z=n,p \\ m:\text{occupied}}} (2j_m+1)\left(\langle m|t_z|m\rangle + \frac{1}{2}\langle m|u_z^{(2)}|m\rangle\right) - \frac{3}{2}\hbar\Omega, \tag{35}$$

where $|m\rangle$ denotes a ho single-particle state for the hole state with a total angular momentum j_m. We also express the unperturbed single-particle energy $E_{\text{sp}}^{(\text{unp})}$ for a state $|a\rangle$ as

$$E_{\text{sp}}^{(\text{unp})} = \langle a|t_z|a\rangle + \langle a|u_z^{(2)}|a\rangle \text{ for } z = n,p. \tag{36}$$

Note that $E_{\text{g.s.}}^{(\text{unp})}$ and $E_{\text{sp}}^{(\text{unp})}$ are implicitly A dependent due to the property of $\tilde{V}_{ij}^{(1)}(A)$ in Eq. (31). We see that the results in Fig. 3 converge when the number of interaction is larger than 4.

C. Diagonalization of the transformed Hamiltonian

The transformed Hamiltonian determined in the second-step calculation does not contain the interaction which induces $2p2h$ excitation. However, there remain some terms inducing $1p1h$ excitation in the one-body Hamiltonian, and coupling terms in the two-body interaction between $1h$ and $1p2h$ states for occupied states, and between $1p$ and $2p1h$ states for unoccupied states. The transformed Hamiltonian to be diagonalized consists of the kinetic and single-particle potential parts, and the two-body effective interaction determined in the second-step calculation. As for the closed-shell nucleus, we diagonalize the transformed Hamiltonian with the shell-model basis states, taking into account $1p1h$ excitation from the unperturbed ground state. We denote the energy shift from the unperturbed energy obtained by the diagonalization by E_{1p1h}. As for the closed-shell nucleus plus one-particle (one-hole) system, the shell-model basis states are composed of the $1p$ and $2p1h$ states ($1h$ and $1p2h$ states). The energy shift from the unperturbed energy obtained by the diagonalization is expressed by E_{2p1h} (E_{1p2h}). The binding energies BE for these systems are given as follows:

$$-BE(^{16}\text{O}) = E_{\text{g.s.}}^{(\text{unp})} + E_{1p1h}, \tag{37}$$

$$-BE(^{17}\text{O},^{17}\text{F}) = E_{\text{g.s.}}^{(\text{unp})} + E_{2p1h}, \tag{38}$$

and

$$-BE(^{15}\text{O},^{15}N) = E_{\text{g.s.}}^{(\text{unp})} + E_{1p2h}. \tag{39}$$

Thus, the single-particle energies E_{sp} for the particle and hole states are written, respectively, as

$$E_{\text{sp}}(^{17}\text{O},^{17}\text{F}) = BE(^{16}\text{O}) - BE(^{17}\text{O},^{17}\text{F}) \tag{40}$$

and

$$E_{\text{sp}}(^{15}\text{O},^{15}N) = BE(^{15}\text{O},^{15}N) - BE(^{16}\text{O}). \tag{41}$$

In the following section, we shall present the calculated results of the energies using Eqs. (35)–(41) with some discussions.

III. RESULTS AND DISCUSSION

In the present study, the number of the ho wave functions which are used as the basis states is finite, and some approximations are made. Therefore, the calculated results have the dependences on the ho energy $\hbar\Omega$ and the value of ρ_1 which specifies the model space in the first-step calculation. In the following sections, some calculated results are shown with the $\hbar\Omega$ and ρ_1 dependences. However, we search for optimal values of $\hbar\Omega$ and values of ρ_1 for which the calculated results almost converge to obtain the final results.

In order to clarify differences in the properties of modern nucleon-nucleon interactions, four interactions represented in momentum space are employed, namely, the Nijm-93, Nijm-I [18], the CD-Bonn [20] and the N^{3}LO [21] potentials, and the Coulomb force is also used commonly. In the calculations, the partial waves up to $J_r \leqq 6$ are taken into account.

A. ^{16}O

In Fig. 4, the $\hbar\Omega$ dependence of calculated ground-state energies of ^{16}O for $\rho_1 = 12$ using the Nijm-93 and the CD-Bonn potentials is shown. The unperturbed energy which is shown as "unp" and the energy with the $1p1h$ correction are displayed separately. The expression of the ground-state en-

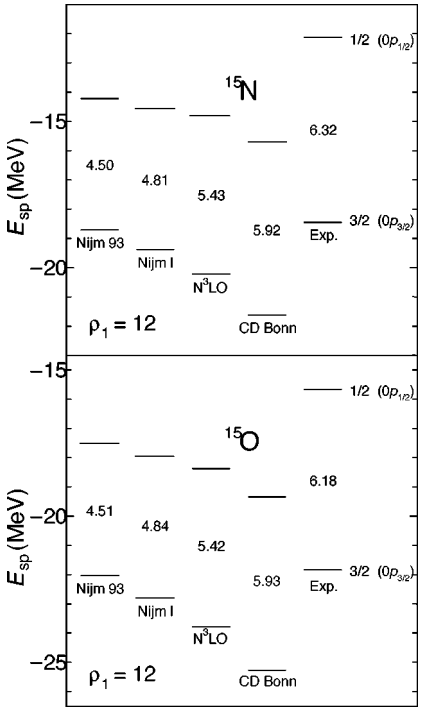

FIG. 8. The calculated single-particle energies with the $1p2h$ effect for $\rho_1=12$ in ^{15}N and ^{15}O. The values of the spin-orbit splitting are also shown. In these calculated values, the optimal values of $\hbar\Omega$ for each single-hole state and interaction are employed.

ergy with the $1p1h$ effect is given in Eq. (37) as $-BE$. We see that the effect of the $1p1h$ correction has a significant contribution attractively to the ground-state energy. If we use the HF wave functions, the unperturbed ground-state energies should become more attractive.

We note here that the values of $\hbar\Omega$ at which the energy minima are obtained differ from each other between the Nijm-93 and the CD-Bonn potentials, and also between the unperturbed and the unperturbed plus $1p1h$ energies, reflecting differences in the properties of the two potentials. In the calculation of ^{16}O, a value around $\hbar\Omega=14$ MeV is often employed as a suitable value of $\hbar\Omega$. This value is very close to that determined by empirical formula such as $\hbar\Omega=45A^{-1/3}-25A^{-2/3}$ MeV. In the present study, however, we regard the value at which the energy minimum is obtained as the optimal one. The optimal value should be searched for each state in nuclei.

Figure 5 illustrates the $\hbar\Omega$ and ρ_1 dependences of the ground-state energy with the $1p1h$ effect for the Nijm-93, Nijm-I, the N^{3}LO, and the CD-Bonn potentials. In principle, we should take the value of ρ_1 as large as possible until the results do not depend on ρ_1. When we take as $\rho_1=14$, the results show fairly good convergence for the CD-Bonn potential. As for the Nijm-93, Nijm-I, and the N^{3}LO potentials, almost convergent results are obtained if we take the value $\rho_1=16$. Note that the energy for $\rho_1=18$ at $\hbar\Omega=14$ MeV is calculated for the N^{3}LO potential in order to confirm the convergence. We see that the results for $\rho_1=16$ and 18 are almost the same.

In Table I, the final results of the ground-state energy with the $1p1h$ effect are tabulated for the four potentials together with the experimental value. The binding energies per nucleon are also shown. The calculated values are for the optimal $\hbar\Omega$ and ρ_1 which can be determined from the results as shown in Fig. 5. The results for the Nijm 93 and the CD Bonn are the least and most attractive, respectively, of the four potentials. This tendency can also be observed in the Faddeev-Yakubovsky calculations for ^{4}He by Nogga *et al.* [33].

TABLE II. The calculated single-particle energies with the $1p2h$ effect for $\rho_1=12$ in ^{15}N. The values of the spin-orbit splitting energy $\Delta E_{ls}(0p)=E_{\rm sp}(0p_{1/2})-E_{\rm sp}(0p_{3/2})$ are also tabulated. In these calculated values, the optimal values of $\hbar\Omega$ for each single-hole state and interaction are employed. The results for $\hbar\Omega=14$ MeV are also shown in parentheses. The experimental values are taken from Ref. [35]. All energies are in MeV.

^{15}N	Nijm 93	Nijm I	N^{3}LO	CD Bonn	Expt.
$1/2^-(0p_{1/2})$	−14.21	−14.56	−14.80	−15.71	−12.13
	(−14.12)	(−14.56)	(−14.80)	(−15.73)	
$3/2^-(0p_{3/2})$	−18.71	−19.37	−20.23	−21.63	−18.45
	(−19.26)	(−19.86)	(−20.17)	(−21.22)	
$\Delta E_{ls}(0p)$	4.50	4.81	5.43	5.92	6.32
	(5.14)	(5.30)	(5.37)	(5.49)	

It is seen that the calculated ground-state energies are less bound than the experimental value. In the present calculation, higher-order correlations such as the three-body cluster terms have not been evaluated. In addition, the real three-body force is not taken into account. The inclusion of the real three-body force and the higher-order many-body correlations would compensate for the discrepancies between the experimental and calculated values. Such a study remains as an important task for a deeper understanding of nuclear ground-state properties in the present approach. A coupled-cluster calculation of the saturation property concerning the binding energy and charge radius for ^{16}O by Mihaila and Heisenberg has shown that the calculated result agrees well with the experimental value when a genuine three-body force is included in the calculation [32].

B. ^{15}N and ^{15}O

Figure 6 shows the $\hbar\Omega$ dependence of calculated single-particle energies for the $0p$ states in ^{15}N and ^{15}O for $\rho_1=12$ in the case of the CD-Bonn potential. The unperturbed

TABLE III. Same as Table II, except for ^{15}O.

^{15}O	Nijm 93	Nijm I	N^{3}LO	CD Bonn	Expt.
$1/2^-(0p_{1/2})$	−17.52	−17.96	−18.37	−19.34	−15.66
	(−17.51)	(−18.00)	(−18.34)	(−19.27)	
$3/2^-(0p_{3/2})$	−22.03	−22.80	−23.79	−25.27	−21.84
	(−22.72)	(−23.37)	(−23.79)	(−24.83)	
$\Delta E_{ls}(0p)$	4.51	4.84	5.42	5.93	6.18
	(5.21)	(5.37)	(5.45)	(5.56)	

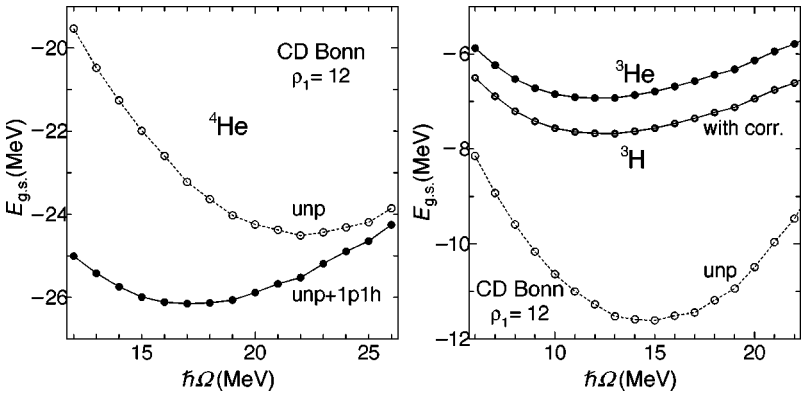

FIG. 9. The $\hbar\Omega$ dependence of calculated ground-state energies of ^{4}He, ^{3}H, and ^{3}He for $\rho_1 = 12$. The CD-Bonn potential is employed.

energy and the energy with the $1p2h$ correction are displayed separately. The unperturbed single-particle energy is given in Eq. (36) and that with the $1p2h$ correction is in Eq. (41). We see that the unperturbed single-particle energies vary considerably at around the typical $\hbar\Omega = 14$ MeV. However, the single-particle energies with the $1p2h$ correction have the saturation points at around $\hbar\Omega \simeq 14-15$ MeV, depending on the single-particle states. Note that the minimum points for the ground-state energies of ^{15}N and ^{15}O correspond to the maximum points of the single-particle energies in Fig. 6. It should be remarked that the spin-orbit splittings for the $0p$ states in ^{15}N and ^{15}O are significantly enlarged by taking into account the $1p2h$ correction. This effect has already been shown in our previous works though the calculation was performed perturbatively by taking into account second-order diagrams on the isospin basis [13,14].

Figure 7 exhibits the $\hbar\Omega$ and ρ_1 dependences of the single-particle energies with the $1p2h$ effect. It is seen that the ρ_1 dependence is weaker than that in Fig. 5. This is because the results in Fig. 6 are the relative values for the binding energies of two nuclei as given in Eq. (41), while those in Fig. 5 are not the relative ones. We may say that, as for the single-particle energies for the hole states, the results for $\rho_1 = 12$ are acceptable as final results in the present study.

In Fig. 8, the final results of the single-particle energies with the $1p2h$ effect for the $0p$ states in ^{15}N and ^{15}O for $\rho_1 = 12$ using the four potentials are shown with the values of the spin-orbit splitting energy. The optimal values of $\hbar\Omega$ for each interaction are searched for the binding energies of ^{16}O, ^{15}N, and ^{15}O in calculating the single-particle energies through Eq. (41). We see that the calculated spin-orbit splittings are smaller than the experimental values though the differences between the calculated and experimental values depend on the nucleon-nucleon interactions employed. The magnitudes of these discrepancies would be reduced if we include a genuine three-body force in the calculation as discussed in Refs. [4,6].

In Tables II and III, the final results of the single-particle energies shown in Fig. 8 are tabulated. The results for the typical $\hbar\Omega = 14$ MeV are also displayed in parentheses for reference. In the case of $\hbar\Omega = 14$ MeV, we use this value commonly in calculating the binding energies of ^{16}O, ^{15}N, and ^{15}O. It is seen that all the calculated single-particle energies are more attractive than the experimental values. The inclusion of the three-body force and the evaluation of higher-order many-body correlations may compensate for the discrepancies between the experimental and calculated values.

In order to see the accuracy of the calculations, it would be worthwhile to apply the present method to the few-nucleon systems ^{4}He, ^{3}H, and ^{3}He as similar systems to ^{16}O, ^{15}N, and ^{15}O. As for the few-nucleon systems, the binding energies have been calculated precisely by various methods [36].

In Fig. 9, the $\hbar\Omega$ dependence of calculated ground-state energies of ^{4}He, ^{3}H, and ^{3}He is shown for $\rho_1 = 12$ using the CD-Bonn potential. The expression of the unperturbed ground-state energy is given in Eq. (35). It is noted that the formulas for calculating the unperturbed ground-state energies of ^{4}He, ^{3}H, and ^{3}He are the same. In these cases, only the $0s_{1/2}$ states of the proton and neutron are regarded as the hole states. However, the results of the unperturbed energies are different between ^{4}He and ^{3}H (^{4}He and ^{3}He) because of the A dependence of the Hamiltonian as given in Eq. (30). The expression of the ground-state energy of ^{4}He with the $1p1h$ correction corresponds to Eq. (37), and that for ^{3}H and ^{3}He with the $1p2h$ effect is similar to Eq. (39). We see that although the calculated results of the unperturbed ground-state energies of ^{3}H and ^{3}He are the same, the energies with the $1p2h$ effect are different because of the charge difference.

In Table IV, the calculated ground-state energies of ^{4}He, ^{3}H, and ^{3}He with the corrections for the optimal values of $\hbar\Omega$ which can be determined from Fig. 9 are tabulated together with the results of the no-core shell model (NCSM) [37,38] and the experimental values. It has been shown that the NCSM results agree well with the results obtained by

TABLE IV. Comparison of the ground-state energies of ^{4}He, ^{3}H, and ^{3}He in the present approximation for $\rho_1 = 12$ with those in the NCSM calculations and the experimental values. The CD-Bonn potential is commonly used in the calculations. The experimental values are taken from Ref. [34]. All energies are in MeV.

	UMOA	NCSM	Expt.
^{3}He	−6.93	−7.25	−7.72
^{3}H	−7.68	−8.00	−8.48
^{4}He	−26.15	−26.30	−28.30
$E_{g.s.}(^3\text{He}) - E_{g.s.}(^3\text{H})$	0.75	0.75	0.76

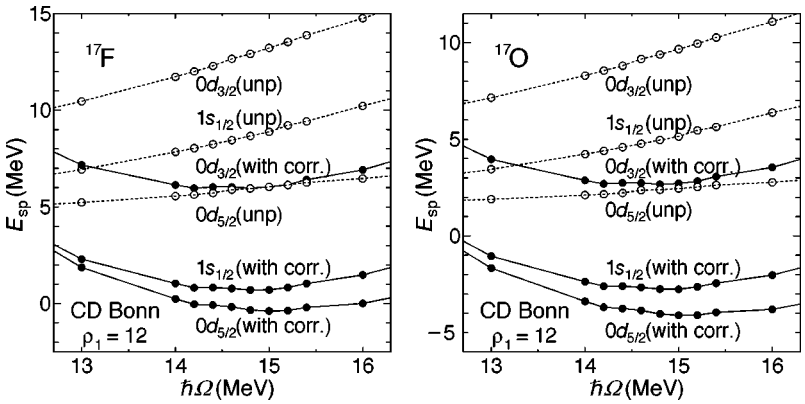

FIG. 10. The $\hbar\Omega$ dependence of calculated single-particle energies for $\rho_1 = 12$ in ^{17}F and ^{17}O. The CD-Bonn potential is employed.

accurate methods for few-nucleon systems such as the Faddeev-Yakubovsky calculation [36]. It is seen that our results are less bound by several hundred keV than the NCSM results. In the present approach, higher-order many-body correlations such as the three-body cluster terms are not taken into account. The evaluation of the higher-order many-body correlations would gain more binding energy. We may say, however, that our result of the charge dependence in the relative energy between ^{3}H and ^{3}He is in good agreement with the NCSM result and also the experimental value.

This kind of agreement of charge dependence can also be seen in the results for ^{15}N and ^{15}O as shown in Tables II and III. The experimental energy difference of the ground states between ^{15}N and ^{15}O is 3.53 MeV. Our result of the energy difference of the single-particle energies for the $0p_{1/2}$ orbits between ^{15}N and ^{15}O is 3.63 MeV for the CD Bonn. One can see that the results for the other potentials also agree well with the experimental value. Thus, we may say that the effect of the Coulomb force for the *pp* channel is correctly treated in our particle-basis formalism. The Coulomb force effect is also discussed in the following section for ^{17}F and ^{17}O.

C. ^{17}F and ^{17}O

Figure 10 shows the $\hbar\Omega$ dependence of calculated single-particle energies for $\rho_1 = 12$ for the 1*s* and 0*d* states in ^{17}F and ^{17}O with the CD-Bonn potential. The unperturbed energy and the energy with the $2p1h$ correction are displayed separately. The definition of the single-particle energy with the correction is given in Eq. (40). We see that all the unperturbed energies are rather unbound and considerably vary at around the typical $\hbar\Omega = 14$ MeV. However, some single-particle states become bound at the energy minimum points by taking account of the corrections. It should be noted that the magnitudes of the spin-orbit splitting with the $2p1h$ effect for the $0d$ states are not very different from those for the unperturbed part at around $\hbar\Omega = 14$ MeV . This tendency differs from the case of the deeply bound hole states for which the $1p2h$ effect plays an important role to enlarge the spin-orbit splittings as shown in Fig. 6.

In Fig. 11, we show the $\hbar\Omega$ and ρ_1 dependences of the single-particle energies with the $2p1h$ effect. We see that the ρ_1 dependence for the $0d_{5/2}$ and $1s_{1/2}$ states shows the good convergence at $\rho_1 = 12$. On the other hand, the results for the $0d_{3/2}$ states do not necessarily converge at $\rho_1 = 12$. Since the $0d_{3/2}$ states of the proton and neutron are highly unbound, it would be necessary to take a larger value of ρ_1 in order to obtain the convergent results. In the present study, however, we employ the values for $\rho_1 = 12$ as the final results of the single-particle energies in ^{17}F and ^{17}O.

Figure 12 shows the final results of the single-particle energies with the $2p1h$ effect in ^{17}F and ^{17}O for the four potentials with the values of the spin-orbit splitting energy. The optimal values of $\hbar\Omega$ are employed for the results. On

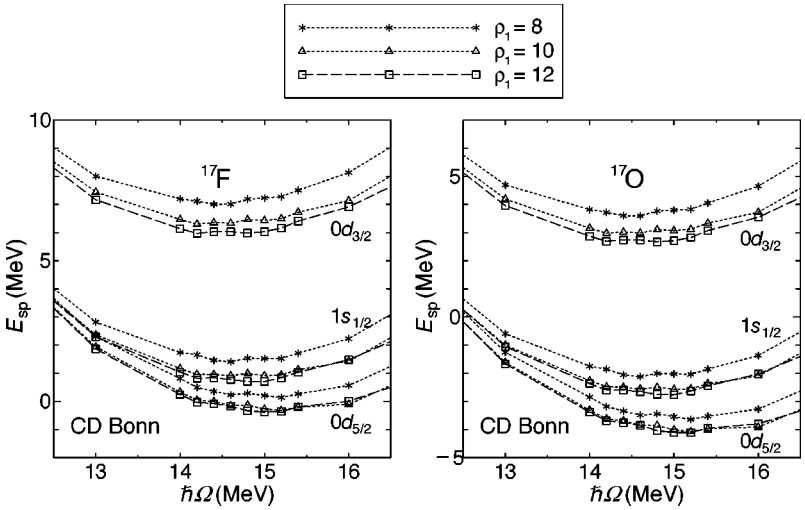

FIG. 11. The $\hbar\Omega$ and ρ_1 dependences of calculated single-particle energies with the $2p1h$ effect in ^{17}F and ^{17}O for the CD-Bonn potential.

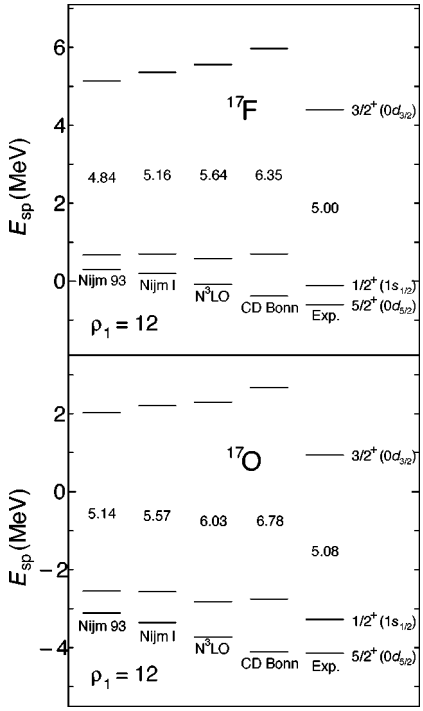

FIG. 12. The calculated single-particle energies with the $2p1h$ effect for $\rho_1=12$ in ^{17}F and ^{17}O for the CD-Bonn potential. The values of the spin-orbit splitting are also shown. In these calculated values, the optimal values of $\hbar\Omega$ for each single-particle state and interaction are employed.

the whole, the calculated spin-orbit energies are larger than the experimental values in contrast to the hole state case. We may say, however, that the calculated results become somewhat smaller if we take a larger value of ρ_1, because the $0d_{3/2}$ states are lowered as suggested in Fig. 11. The calculated results for the ground $0d_{5/2}$ states agree fairly well with the experimental values in contrast to the results for the ground $0p_{1/2}$ states in ^{15}N and ^{15}O. However we note that, in our preliminary estimation, the three-body cluster effect for the particle state shows a repulsive contribution significantly to the single-particle energy if only the two-body interaction is employed [40].

In Tables V and VI, the final results of the single-particle energies shown in Fig. 12 are tabulated together with the spin-orbit splitting energies for the $0d$ states and the energy differences between the $1s_{1/2}$ and $0d_{5/2}$ states. The values for the typical $\hbar\Omega=14$ MeV are also displayed in parentheses for reference. We may say that our results for the magnitudes of these two splittings are not very different from the experimental values. However, we should take account of the real three-body force and evaluate higher-order many-body correction terms to obtain more reliable results. This kind of study is in progress.

We here discuss effects of the Coulomb force. The experimental mass difference between ^{17}F and ^{17}O is 3.54 MeV. The calculated results lie between 3.41 and 3.73 MeV for the four potentials in the case of the optimal $\hbar\Omega$ and between 3.50 and 3.63 MeV in the case of $\hbar\Omega=14$ MeV as seen from the values in Tables V and VI. These calculated values are in good agreement with the experimental value. This kind of

TABLE V. The calculated single-particle energies with the $2p1h$ effect for $\rho_1=12$ in ^{17}F. The values of the spin-orbit splitting energy $\Delta E_{ls}(0d)=E_{\rm sp}(0d_{3/2})-E_{\rm sp}(0d_{5/2})$ and the energy differences between the $1s_{1/2}$ and $0d_{5/2}$ states $\Delta E_{sd}=E_{\rm sp}(1s_{1/2})-E_{\rm sp}(0d_{5/2})$ are also tabulated. In these calculated values, the optimal values of $\hbar\Omega$ for each single-particle state and interaction are employed. The results for $\hbar\Omega=14$ MeV are also shown in parentheses. The experimental values are taken from Ref. [39]. All energies are in MeV.

^{17}F	Nijm 93	Nijm I	N^{3}LO	CD Bonn	Expt.
$3/2^+(0d_{3/2})$	5.14	5.36	5.56	5.97	4.40
	(5.50)	(5.66)	(5.43)	(5.63)	
$1/2^+(1s_{1/2})$	0.67	0.70	0.58	0.70	−0.11
	(0.84)	(0.83)	(0.52)	(0.54)	
$5/2^+(0d_{5/2})$	0.30	0.20	−0.08	−0.38	−0.60
	(0.22)	(0.21)	(−0.05)	(−0.26)	
ΔE_{sd}	0.37	0.50	0.66	1.08	0.49
	(0.62)	(0.62)	(0.57)	(0.80)	
$\Delta E_{ls}(0d)$	4.84	5.16	5.64	6.35	5.00
	(5.28)	(5.45)	(5.48)	(5.89)	

agreement has been shown also for the hole states. Furthermore, another effect of the Coulomb force appears in the particle states. The experimental $1s_{1/2}$ states of the proton and neutron lie above the $0d_{5/2}$ states by 0.49 and 0.87 MeV in energy, respectively. Thus, the $1s_{1/2}$ state in ^{17}F is close to the $0d_{5/2}$ state by 0.38 MeV than in ^{17}O. This effect is known as the Thomas-Ehrman shift due to the Coulomb force [41–44]. In our results, the magnitudes of the shift are from 0.19 to 0.29 MeV for the cases of the optimal $\hbar\Omega$ and from 0.22 to 0.23 MeV for $\hbar\Omega=14$ MeV, depending on the interactions employed. In the latter case the results hardly depend on the potentials, because the unperturbed $1s_{1/2}$ ho wave functions are the same for all the cases using the four interactions, and thus the Coulomb force works equally in the calculations. Although some discrepancies between the experimental and calculated values are seen, we may say that the Thomas-Ehrman effect can be observed in our results.

IV. SUMMARY AND CONCLUSIONS

The method for calculating the ground-state energy and single-particle energy has been developed within the frame-

TABLE VI. Same as Table V, except for ^{17}O.

^{17}O	Nijm 93	Nijm I	N^{3}LO	CD Bonn	Expt.
$3/2^+(0d_{3/2})$	2.03	2.21	2.30	2.67	0.94
	(2.33)	(2.47)	(2.19)	(2.37)	
$1/2^+(1s_{1/2})$	−2.55	−2.57	−2.82	−2.76	−3.27
	(−2.43)	(−2.49)	(−2.86)	(−2.87)	
$5/2^+(0d_{5/2})$	−3.11	−3.36	−3.73	−4.11	−4.14
	(−3.28)	(−3.33)	(−3.66)	(−3.89)	
ΔE_{sd}	0.56	0.79	0.91	1.35	0.87
	(0.85)	(0.84)	(0.80)	(1.02)	
$\Delta E_{ls}(0d)$	5.14	5.57	6.03	6.78	5.08
	(5.61)	(5.80)	(5.85)	(6.26)	

work of the unitary-model-operator approach (UMOA). The expressions for the numerical calculation have been recast from the isospin basis to the particle one for the charge-dependent structure calculation. We have applied the UMOA to ^{16}O, ^{15}N, ^{15}O, ^{17}F, and ^{17}O employing modern nucleon-nucleon interactions, such as the Nijm-93, Nijm-I, the CD-Bonn, and the N^{3}LO potentials which have charge dependence. The Coulomb force has been also used for the *pp* channel. In order to obtain the final results, we have searched for the optimal values of $\hbar\Omega$ and the values of ρ_1 for which the calculated results almost converge.

The accuracy of the approximation in the present method has been investigated by calculating the ground-state energies of ^{4}He, ^{3}H, and ^{3}He and comparing the present results with the accurate no-core shell-model (NCSM) results. We have found that the energy differences between the NCSM and our results for these systems are several hundred keV for the CD-Bonn potential. As for the energy difference between ^{3}H and ^{3}He, our result agrees well with the NCSM result and the experimental value.

The good agreement for charge dependence between the present results and the experimental values is observed also in the differences in the ground-state energies between ^{15}N and ^{15}O, and ^{17}F and ^{17}O. The effect of charge dependence is also seen in the Thomas-Ehrman shift for the $1s_{1/2}$ states in ^{17}F and ^{17}O.

We have shown that the calculated spin-orbit splittings for the $0p$ hole states are enlarged significantly by taking the $1p2h$ effect into account, and become close to the experimental value. On the other hand, the influence of the inclusion of the $2p1h$ effect on the spin-orbit splittings for the $0d$ particle states is rather small. On the whole, the calculated spin-orbit splittings for the hole and particle states in nuclei around ^{16}O are not very different from the experimental values though the results somewhat depend on the interactions employed.

In the present work, higher-order many-body correlations such as the three-body cluster terms are not evaluated. In addition, the real three-body force is not included in the calculations. We should take account of these effects for a deeper understanding of the nuclear structure.

By virtue of the extension of the calculation method to the particle basis, the present method can be applied to proton- or neutron-rich nuclei in the same manner. The mechanism of the variation of magic numbers near the drip lines may be clarified from a microscopic point of view. The study of neutron-rich nuclei around ^{24}O is in progress. Results for these systems will be reported elsewhere in the near future.

ACKNOWLEDGMENTS

The authors are grateful to D. R. Entem for providing us the charge-dependent N^{3}LO potential code in reply to our request. One of the authors (S.F.) acknowledges the Special Postdoctoral Researchers Program of RIKEN. This work was supported by a Grant-in-Aid for Scientific Research (C) from Japan Society for the Promotion of Science (JSPS) (Grant No. 15540280).

[1] A. Ozawa, T. Kobayashi, T. Suzuki, K. Yoshida, and I. Tanihata, Phys. Rev. Lett. **84**, 5493 (2000).
[2] T. Otsuka, R. Fujimoto, Y. Utsuno, B. A. Brown, M. Honma, and T. Mizusaki, Phys. Rev. Lett. **87**, 082502 (2001).
[3] H. Kümmel, K. H. Lührmann, and J. G. Zabolitzky, Phys. Rep., Phys. Lett. **36**, 1 (1978).
[4] K. Andō and H. Bandō, Prog. Theor. Phys. **66**, 227 (1981).
[5] L. Zamick, D. C. Zheng, and H. Müther, Phys. Rev. C **45**, 2763 (1992).
[6] S. C. Pieper and V. R. Pandharipande, Phys. Rev. Lett. **70**, 2541 (1993).
[7] H. Müther and A. Polls, Prog. Part. Nucl. Phys. **45**, 243 (2000), and references therein.
[8] T. T. S. Kuo and E. Osnes, *Folded-Diagram Theory of the Effective Interaction in Nuclei, Atoms and Molecules*, Lecture Notes in Physics Vol. 364 (Springer, Berlin, 1990), and references therein.
[9] M. Hjorth-Jensen, T. T. S. Kuo, and E. Osnes, Phys. Rep. **261**, 125 (1995), and references therein.
[10] Kh. Gad and H. Müther, Phys. Rev. C **66**, 044301 (2002).
[11] S. K. Bogner, T. T. S. Kuo, and A. Schwenk, Phys. Rep. **386**, 1 (2003).
[12] L. Coraggio, N. Itaco, A. Covello, A. Gargano, and T. T. S. Kuo, Phys. Rev. C **68**, 034320 (2003).
[13] K. Suzuki and R. Okamoto, Prog. Theor. Phys. **92**, 1045 (1994).
[14] K. Suzuki, R. Okamoto, and H. Kumagai, Phys. Rev. C **36**, 804 (1987).
[15] H. Kumagai, K. Suzuki, and R. Okamoto, Prog. Theor. Phys. **97**, 1023 (1997).
[16] S. Fujii, R. Okamoto, and K. Suzuki, Prog. Theor. Phys. **104**, 123 (2000).
[17] S. Fujii, R. Okamoto, and K. Suzuki, Phys. Rev. C **66**, 054301 (2002).
[18] V. G. J. Stoks, R. A. M. Klomp, C. P. F. Terheggen, and J. J. de Swart, Phys. Rev. C **49**, 2950 (1994).
[19] The original versions of the Nijmegen potentials are constructed in configuration space. We use the momentum-space versions which can be downloaded from the NN-OnLine homepage at http://nn-online.sci.kun.nl/
[20] R. Machleidt, F. Sammarruca, and Y. Song, Phys. Rev. C **53**, R1483 (1996).
[21] D. R. Entem and R. Machleidt, Phys. Rev. C **68**, 041001 (2003).
[22] S. Weinberg, Phys. Lett. B **251**, 288 (1990); Nucl. Phys. **B363**, 3 (1991).
[23] C. Ordóñez, L. Ray, and U. van Kolck, Phys. Rev. Lett. **72**, 1982 (1994); Phys. Rev. C **53**, 2086 (1996).
[24] K. Suzuki, Prog. Theor. Phys. **68**, 246 (1982).
[25] S. Ōkubo, Prog. Theor. Phys. **12**, 603 (1954).
[26] J. P. Jeukenne, A. Lejeune, and C. Mahaux, Phys. Rep., Phys. Lett. **25**, 83 (1976).

[27] T. T. S. Kuo, Z. Y. Ma, and R. Vinh Mau, Phys. Rev. C **33**, 717 (1986).
[28] K. Suzuki, R. Okamoto, and H. Kumagai, Prog. Theor. Phys. **77**, 196 (1987).
[29] H. Q. Song, M. Baldo, G. Giansiracusa, and U. Lombardo, Phys. Rev. Lett. **81**, 1584 (1998).
[30] C. W. Wong, Nucl. Phys. **A91**, 399 (1967).
[31] D. J. Dean, M. T. Ressell, M. Hjorth-Jensen, S. E. Koonin, K. Langanke, and A. P. Zuker, Phys. Rev. C **59**, 2474 (1999).
[32] B. Mihaila and J. H. Heisenberg, Phys. Rev. C **61**, 054309 (2000).
[33] A. Nogga, H. Kamada, W. Glöckle, and B. R. Barrett, Phys. Rev. C **65**, 054003 (2002).
[34] G. Audi and A. H. Wapstra, Nucl. Phys. **A565**, 1 (1993).
[35] F. Ajzenberg-Selove, Nucl. Phys. **A523**, 1 (1991).
[36] H. Kamada *et al.*, Phys. Rev. C **64**, 044001 (2001).
[37] P. Navrátil, G. P. Kamuntavičius, and B. R. Barrett, Phys. Rev. C **61**, 044001 (2000).
[38] P. Navrátil, J. P. Vary, W. E. Ormand, and B. R. Barrett, Phys. Rev. Lett. **87**, 172502 (2001).
[39] D. R. Tilley, H. R. Weller, and C. M. Cheves, Nucl. Phys. **A564**, 1 (1993).
[40] S. Fujii, R. Okamoto, and K. Suzuki, nucl-th/0312107.
[41] J. B. Ehrman, Phys. Rev. **81**, 412 (1951).
[42] R. G. Thomas, Phys. Rev. **88**, 1109 (1952).
[43] S. Aoyama, N. Itagaki, K. Kato, and K. Ikeda, Phys. Rev. C **57**, 975 (1998).
[44] K. Ogawa, H. Nakada, S. Hino, and R. Motegi, Phys. Lett. B **464**, 157 (1999).